JOURNAL OF PHYSICAL CHEMISTRY A (ISSN: 1089-5639) (eISSN: 1520-5215) 119(50): 12485-12497 (2015)

DOI: 10.1021/acs.jpca.5b07938

The Dynamics of Complex-Forming Bimolecular Reactions: a Comparative Theoretical Study of the Reactions of H atoms with $O_2(^3\Sigma_g^-)$ and $O_2(^1\Delta_g)$

Péter Szabó[1] and György Lendvay[1,2]*

[1]Department of General and Inorganic Chemistry, Institute of Chemistry, University of Pannonia, P.O.B. 158, Veszprém H-8201, [2]Institute of Materials and Environmental Chemistry, Research Centre for Natural Sciences, Hungarian Academy of Sciences, Budapest, Magyar Tudósok krt. 2., H-1117 Hungary

* To whom correspondence should be addressed. E-mail: lendvay.gyorgy@ttk.mta.hu

Abstract The atomic-level mechanism of the reaction of H atoms with triplet and singlet molecular oxygen, $H(^2S) + O_2(^3\Sigma_g^-) \rightarrow O(^3P) + OH(^2\Pi_g)$ (R1) and $H(^2S) + O_2(^1\Delta_g) \rightarrow O(^3P) + OH(^2\Pi_g)$ (R2) is analyzed in terms of the topology of the potential energy surfaces (PES) of the two reactions. Both PES exhibit a deep potential well corresponding to the ground- and first excited electronic state of HO_2. The ground-state reaction is endothermic with no barrier on either side of the well; the excited-state reaction is exothermic with a barrier in the entrance valley of the PES. The differences of the PES are manifested in properties such as the excitation functions, which show reaction R1 to be much slower and the effect of

rotational excitation on reactivity, which speeds up reaction R1 and has little effect on R2. Numerous common dynamics features arise from the presence of the deep potential well on the PES. Such are the significant role of isomerization (for example, 90% of reactive collisions in R2 involve at least one H atom transfer from one of the O atoms to the other in reaction R2) which is shown to give rise to a significant rotational excitation of the product OH radicals. Common is the significant sideways scattering of the products that originates from collisions in propeller-type arrangements induced by the presence of two bands of acceptance around the O_2 molecule. The HO_2 complex in both reactions proves to behave non-statistically, with signatures of the dynamics in lifetime distributions, angular distributions, opacity functions and product quantum state distributions.

INTRODUCTION

Reaction dynamics experiments and modeling has been in the focus of chemist's attention since the 1930's, because they provide information about the course of chemical reactions at the atomic level. The discovery of the potential barrier on the H + H_2 potential surface by Eyring and M. Polanyi shed light[1] on the origin of the activation energy Arrhenius introduced decades earlier, without any convincing explanation. Polanyi[2] also strived to understand the reasons why some reactions produce vibrationally excited products while others did not. Experiments can provide a lot of valuable, but generally incomplete information on reaction dynamics, so it is not only fruitful but also necessary to apply theoretical approaches to complement and interpret the experimental information. The field became one of the nicest examples where experiment and theory can, step by step, make a clear picture of the studied phenomenon. The basic concept in modeling reaction dynamics is the Born-Oppenheimer approximation, separating electronic and nuclear motion. The solution of the electronic Schrödinger equation provides a stationary multidimensional potential energy surface (PES)

that formally provides the forces governing the motion of atoms represented by their nuclei. Then the only thing to be done is to solve the nuclear equations of motion preferably using quantum mechanics, or, relying on the relatively large mass of nuclei, classically. The technology for numerical simulation of molecular collisions using classical mechanics has been available since Newton, Lagrange, Euler and others, only the potential surface provided by the electronic Schrödinger equation is needed. This was missing until about the last decade (and partially the previous one[3]) when full-dimensional PES calculated by reasonably accurate ab initio calculations have been worked out. The quantum mechanical technology to describe quantum effects in molecular collisions developed in the 1970's and by now, full-dimensional quantum mechanical calculations appeared for the H + CH_4 reaction[4].

Before reliable potential surfaces became available, empirical potential surfaces adjustable at will were used in classical trajectory calculations. A prominent example is the work led by J.C. Polanyi, culminating in the discovery of the rules named after him, which was based on adjustable analytical LEPS type potential energy surfaces, one of the purposes being to derive principles and qualitative rules governing chemical reactions. With the advent of good ab initio potential energy surfaces, this aspect went out of the focus of most theoreticians, the guiding principle being the development of better dynamical methods and reaching better and better agreement with experiment. This is partly understandable since ab initio potential energy surfaces are "rigid"; it is hard to modify them to change their characteristics. However, there are systems similar to each other for which reliable ab initio potential surfaces are available with clearly characterized differences in their topology. Such is the H + O_2 reaction, which has been a subject of extensive studies. The reaction of O_2 in ground electronic state is endothermic to yield O + OH, that of the electronically excited molecule is exothermic but goes through a potential barrier to produce the same pair of products (a more

detailed analysis follows below). We intend to utilize this advantageous situation and figure out how some specific differences in the PES are manifested in the dynamics of the reaction.

The reason why the selected reaction has been studied so exhaustively is that it is a key reaction in combustion.[5,6]. In addition to extensive reaction kinetics work[7,8,9,10,11,12,13,14,15,], numerous theoretical studies[,16,17,18,19,20,21,22,23,24,25,26,27,28,29,30] have been performed to describe the dynamics of the reaction of ground-state molecular oxygen,

$H(^2S) + O_2(^3\Sigma_g^-) \square O(^3P) + OH(^2\Pi_g)$. (R1)

and recently the kinetics[31,32,33,34,35,36] and dynamics[37,38,39] of the reaction of electronically excited molecular oxygen, $O_2(^1\Delta_g)$ with H atoms,

$H(^2S) + O_2(^1\Delta_g) \square O(^3P) + OH(^2\Pi_g)$ (R2)

has also been explored. The thermal rate coefficients calculated from the excitation functions agree well with the experiments. Both reactions represent the class of complex-forming bimolecular reactions.[40,] Although there is a deep potential well on both the ground- and excited state potential energy surface (PES), both reactions were found[25,38,39,41,42] to display non-statistical behavior, especially at higher collision energies.

The potential energy surfaces of the two reactions differ significantly beyond the common feature, a potential well corresponding to stable HO_2 (see Fig. 1.) Namely, the ground-state reaction is endoergic by 51.2 kJ/mol (classical energy difference), setting the lower limit to reaction at a relatively high energy. On the other hand, in the exited state, the reaction is exoergic by 41.5 kJ/mol and the energetic threshold is determined by the relatively low barrier in the entrance channel (the classical height of which is 31.7 kJ/mol). Electronic excitation has been found to significantly increase the reactivity of O_2 towards H atoms[39]. In accordance with the expectations based on the endoergicity of reaction R1 and the barrier height of reaction R2, the excitation functions are characterized by a threshold energy near 58 kJ/mol and 30 kJ/mol, respectively for R1 and R2, when the reactant diatom is in vib-

rotational ground state. (see Fig. 2.). The electronically excited oxygen is much more reactive than the ground-state molecule. Two factors contribute to the enhancement of the reactivity: for H + $O_2(^1\Delta_g)$ i) the threshold energy is much lower and ii) the cross sections increase faster starting from the threshold and remain much larger in the whole reactive range of collision energy than when O_2 is in the ground state. Due to this effect the rate of reaction R2 is larger by orders of magnitude, which has been discussed in Ref. 39. Numerous features of the ground-state reaction have been detected that indicate non-statistical behavior.[19,25,40] Dynamics was also found to be dictated by the shape of the PES[39] in reaction R2. For example, Polanyi's rule applies to the reaction, namely, on the early-barrier PES, vibrational excitation of the reactant diatom is not favorable for enhancing the reactivity. The complexes formed, even when having relatively long lifetimes, were found to disobey several expectations for the applicability of statistical rate theories. First, in the majority of collisions, the system, after entering the potential well, cross the potential barrier twice, once on the way in, once on the way back to reactants[39]. Second, the lifetime distribution of the complex is not exponential in contrast to the requirements of the applicability of statistical theories. Third, the lifetime distribution and the outcome of collisions varies according to the nature of the degree of freedom (vibration, rotation, translation) in which the energy is made available for the system. Some of these features have also been explored for reaction R1[18,19,25,28,29,43], but no systematic comparison has been made, especially not concerning the differences between other dynamical observables for the two reactions.

The difference between the PES of reactions R1 and R2 offers a unique opportunity to study the fingerprints of various features of the PES on different experimental and calculated dynamical properties. The purpose of our work was to explore what is common and what is different in the two reactions. In the following, after a brief summary of methodology, we present the comparison of the dynamics of reactions R1 and R2 at successively deeper levels:

influence of rotational excitation of the reactant O_2 on the excitation functions; product state distributions including those for nonreactive collisions; the lifetime distributions of the collision complexes; the role of isomerization within the complex in the microscopic mechanism of the reaction and the factors influencing the stereodynamics of the reaction, and discuss how these features are influenced by the shape of the PES.

METHODS

The reaction dynamics were studied using the quasiclassical trajectory (QCT) method. The calculations were performed using an extensively modified version of the VENUS code[44]. 2×10^5 trajectories were calculated at each collision energy. The details of the setting of the remaining parameters are the same as described in Ref. 39. Briefly, the potential surfaces developed by Xu *et al*. (XXZLG)[45] (see Refs. 19, 26 for improvements) and by Li *et al*. (LXDJMG)[37] were used for reaction R1 and R2, respectively. The derivatives of both potential energy surfaces are discontinuous at the C_{2v} arrangement. Since this may distort the outcome of trajectories and destroy energy conservation along trajectories, we tested a smoothing technique similar to the symmetrization proposed by Dawes *et al.*[46] The details of our method are summarized in the Appendix. We found that, while individual trajectories changed their course in some cases if they happened to visit the C_{2v} region, the ensemble average cross sections, angular and product state distributions and even the fraction of isomerized trajectories (see below) remained the same as with the original PES. Since with the smoothed PES we needed to use numerical derivatives, the calculations were much less productive, so in the bulk of the calculations we used the original XXZLG and LXDJMG routines. We found that energy conservation is violated in less than 0.1% of the integrated trajectories, and discarded them.

The reaction and capture probabilities and cross sections were evaluated by the Gauss-weighted QCT method[47,48,49] using a width parameter 0.05. The occurrence of complex formation was detected for each trajectory (irrespectively whether reactive or nonreactive) in

the following way. For both reactions R1 and R2, when the potential energy of the system decreased below one half of the dissociation energy to the O + OH product, the trajectory was considered complex-forming. This is a rather conservative estimate for capture (it should be noted that variation of the energy criterion up by as much as 40 kJ/mol did not induce significant changes in the calculated fraction of complex-forming trajectories). The stereodynamics of the reaction were studied by fixing the orientation of the angular momentum of O_2 with respect to the plane determined by the initial orbital angular momentum as well as the initial velocity vector (see the details below). The lifetime of the collision complex was defined as the classical analog of Smith's lifetime matrix,[50] namely, as the delay induced by the interaction. It was calculated as the difference between the total time of the collision and the sum of the times of the free inbound and outbound flights before and after the reaction (or after a nonreactive encounter). The inbound flight time is calculated from the difference of the initial center-of-mass distance and the hard-sphere diameter (selected to be 3 Å) using the initial relative speed, that of the outbound flight the same way using the final relative speed and the appropriate reduced mass. The value of the hard-sphere diameter is arbitrary, but as long as it is large enough, small changes only shift the calculated lifetime of the collision complex but not the shape of the lifetime distribution. Additional details on the microscopic mechanism were obtained by counting and recording various events such as isomerization, when the H atom switches from one O atom to the other.

The error bars calculated using the standard Monte Carlo formula are of the size of the symbols in the figures and are not plotted.

RESULTS

A. Comparison of the role of rotational excitation of reactants on the excitation functions of the reaction of H atoms with of $O_2(^3\Sigma_g^-)$ and with $O_2(^1\Delta_g)$ Insight into the

dynamics is provided by the influence of rotational and vibrational excitation of O_2 on the reactivity. The effect of vibrational excitation has been found to be limited in both electronic states. The influence of placing energy into O_2 rotation shows remarkable differences between reactions R1 and R2, reflected in the changes of the excitation functions presented in Fig. 2. (Note that, due to nuclear symmetry, $O_2(^3\Sigma_g^-)$ has only odd, $O_2(^1\Delta_g)$ only even rotational states). As discussed in Ref. 39, on the excited-state potential surface the reactivity is only slightly enhanced: the threshold energy decreases by less than 9 kJ/mol even when 60 rotational quanta (corresponding to as much as about 62 kJ/mol) are deposited in the reactant diatom and the cross sections are only slightly larger than with rotationally unexcited O_2. The reduction of the threshold energy is negligible as compared with the rotational energy added to the system, and is not proportional to it, as well as the slope of the excitation functions also vary with the rotational quantum number of O_2. The situation is different for the reaction R1 of ground-state O_2 where the threshold energy decreases significantly, by about 75 % of the rotational energy of the oxygen, and the cross sections are much larger at a given collision energy when *j* is large. An approximation similar to *J*-shifting does not work precisely for this reaction, either: the shift of the threshold is not identical to the extra energy provided in rotation and the shape of the excitation function is also different for different O_2 rotational states. The difference of the effect of reactant rotational excitation for the two reactions deserves a detailed investigation.

Since the prerequisite for reaction in both electronic states is that the system enters the potential well, the mechanism of the reaction can be thought of capture as the first step (even if the complex is not long-lived) and decomposition to O +OH (or back to H + O_2) as the second. Analysis of the two steps can help one to understand the mechanism induced by the two different potential energy surfaces. Fig. 3. shows how the opacity functions for capture (i.e., complex formation as defined in the Methods section) as well as for reaction vary when

the collision energy and the initial angular momentum of O_2 changes. In the ground-state reaction (Fig. 3a) the opacity function for complex formation is insensitive to the rotational state of O_2. This means that in reaction R1, irrespectively whether the O_2 molecule rotates slowly or fast, the H atom finds its way to the potential well with the same efficiency. The enhancement of the reactivity due to rotational excitation is then a consequence of the processes within the complex. The system, after entering the well, spends a relatively long time within it (especially at lower collision energy), allowing room for energy exchange between modes. The fact that the reduction of the collision energy threshold for reaction is almost as large as the additional energy supplied to the system in the form of rotation suggests that almost all rotational energy is utilized for inducing reaction. The primary effect of rotational excitation is that it provides more energy that the HO_2 complex can utilize for decomposition into O + OH. The efficiency of rotational energy in inducing reaction is emphasized by the observation that well above threshold, the reaction cross sections for rotationally excited reactants are much larger than when the same amount of energy is provided in the form of collisional energy. This means that when the collision energy is also large, rotational energy is more efficiently converted to that of the O-O stretch, (which is obviously the critical coordinate for the decomposition of HO_2) than at lower collision energy. In simple terms, rotational excitation of O_2 enhances the reaction cross sections by facilitating the decomposition step and does not influence the efficiency of the complex formation step.

The picture is different for the reaction of singlet oxygen. In reaction R2, the probabilities of complex formation, of product formation ("reactive") and of formation and dissociation of the complex back to reactants ("nonreactive") all increase at low collision energy with rotational excitation of the O_2 reactant (red vs. black symbols in Fig. 3b). At large collision energy only the probability of reactive complex-forming events increases appreciably due to

the extra rotational energy in O_2 (blue vs. green symbols), the contribution of nonreactive complex-forming events does not change. The effect of rotation then is that at low collision energy it promotes the complex formation, and the enhanced reactivity is now a consequence of the enlarged efficiency of the first reaction "step". In terms of the potential energy surface, the rotation of O_2 increases the probability of complex formation, especially at low E_{coll} by making easier the crossing the entrance barrier. On the other hand, the extra energy that the O_2 rotation brings into the complex plays a secondary role. It does not help significantly the decomposition of the complex into products, which is easy to understand considering that the reaction is exothermic. Any effect the reactant rotation causes in this step is because of angular momentum conservation.

Note that the role of the reduction of the centrifugal barrier at a fixed total angular momentum has also been proposed to explain the favorable effect of reactant rotation on reactivity in reaction R1.[43] However, the fact that the effect is observable when the reaction probabilities are averaged over the impact parameter suggests that the intermode energy exchange and the larger available energy provided by O_2 rotation plays a more important role.

B. Energy disposal The product state distributions also reflect the common features and the differences between the PESs of the two reactions. Fig. 4 shows the vibrationally resolved OH rotational distributions for reactions a) R1 and b) R2. (Note that since we do not make comparisons with experimental rotational distributions, the OH radical is treated as a $^1\Sigma$ molecule and the coupling between rotational and electronic orbital angular momenta[51,52] is disregarded). In reaction R1 the OH radical is formed in the ground vibrational state even at high collision energies, because the available energy is small due to the endoergicity of the reaction. In reaction R2, on the other hand, there is ample energy available for the products after the reaction so that OH radicals can carry two or more vibrational quanta depending on

the collision energy (the reaction energy itself covers as much as two vibrational quanta), generating more vibrationally excited OH molecules than what would correspond to a thermal distribution. A common feature is that the products are formed rotationally highly excited in both reactions R1 and R2 already at low collision energies, inducing rotational population inversion (that will very quickly get thermalized in a collisional environment). We return to the dynamical reason for the high OH rotational excitation in Section E.

It is remarkable that in reaction R2 there is a large number of nonreactive collisions visiting the deep HO_2 potential well but leave it very quickly, even at relatively low collision energies. These collisions are not "innocent" in the sense that there is a large energy exchange between the partners. Fig. 5 shows the vibrational distribution of O_2 after complex-forming collisions in R2 starting from the ground vibrational state. As soon as there is enough energy to excite vibration, a large fraction of O_2 molecules gain one or more vibrational quantum. The O_2 also gains significant rotational excitation. Significant energy exchange is also observable for reaction R1 but there it is not surprising since the complex is formed without a barrier and, the reaction being endothermic, the majority of capture events will lead to re-formation of reactants. Because of this, the analysis below focuses on collisions of $O_2(^1\Delta_g)$ with H atoms.

The majority of O_2–H collisions are nonreactive and in most cases the H atom is bounced back from the external repulsive wall of the PES. These are also very quick events. Analyzing the energy content of O_2 after collisions in which no complex is formed, we found no sign of appreciable vibrational excitation. A small fraction of O_2 molecules gain some rotational energy, but there is no T–V energy transfer even at high collision energy. The energy transfer is much more efficient in short-lived complex-forming collisions than in non-complex-forming collisions. There is no significant difference between the vibrational energy distributions of O_2 after very short-lived and long-lived complex-forming collisions or

whether isomerization takes place within the HO_2 potential well. This means that even when there is not enough time for energy equilibration within the complex, the efficiency of the energy transfer is much larger than when the transfer occurs in the external repulsive domain of the PES. Similar phenomenon has been observed in the $H+H_2O$ reaction[53] where frustrated reactive collisions proved to be much more efficient in energy transfer than when the H atom was repelled from the external wall of the PES. Entering the strong interaction region abruptly increases the efficiency of energy transfer no matter whether the collision partner penetrates a potential well characterizing a stable species ($H+O_2$) or approaches a potential barrier of a bimolecular reaction in the nonbound regime ($H+H_2O$). The importance of this effect is rarely noticed, but it is reasonable to assume that in complex reaction systems, nonequilibrium energy distribution can be produced by nonreactive collisions of reactive partners. For example, in combustion systems, $H–O_2$ collisions can generate vibrationally significantly excited O_2 molecules whose reactivity is enhanced with respect to thermal O_2.

C. Lifetime distributions of collision complexes In Fig. 6 the lifetime distributions of the collision complexes in which the system enters the potential well and produce reactive and nonreactive products, respectively, are shown for reaction a) R1 and b) R2 (the detailed definition of complex formation and lifetime is given in the Methods section). The two collision energies selected are: a low one slightly above the respective threshold and a high one. Those collisions in which the H atom does not enter the deep potential well are fast and would all fall in the first lifetime bin. Such collisions have been excluded when the lifetime distributions were calculated. In all cases, in a large fraction of collisions (60 to 90%) the lifetime of the collision complex is small, less than 0.5 ps. This lifetime is not enough to randomize the energy between the degrees of freedom of HO_2. Above about 1 ps the lifetime distributions approach exponential (linear in the semilogarithmic plot of Fig. 6),

corresponding to what is expected for a statistical complex. However, neither reaction R1 nor R2 shows perfect statistical behavior at any collision energy. Common in the two distributions is that the magnitudes of the slopes of the lifetime distributions for both reactive (closed triangles vs. squares) and nonreactive (open triangles vs. squares) collisions increase significantly when the collision energy increases, but in reaction R2 this tendency is appreciable only in the longer collision lifetime region. Furthermore, in the longer than 0.5ps domain, in reaction R1 at a given collision energy, the slopes of the reactive and nonreactive collision lifetime distributions are very similar (the decay rates are the same within a factor of two). In contrast, in reaction R2 at low E_{coll} the decay of the collision complexes is slower for reactive than for nonreactive collisions, but when the collision energy increases, the difference of decay rates gradually decreases and eventually not only the slopes become similar, but the decay curves approach each other and above 96 kJ/mol they in fact almost overlap.

The speed-up of the decay with increasing E_{coll} is an expected phenomenon. The initial slope for the nonreactive collisions increases since the encounters in which no reaction happens and the partners just touch each other and are reflected from the inner wall of the potential well will last shorter when the relative velocity is larger. Concerning reactive events, the more energy is available the faster reaction is expected. The effect is more clearly manifested in the longer, 1 or 2 ps lifetime range where the complexes live long enough for efficient energy exchange between modes. These expectations are qualitatively fulfilled by both reactions.

The similarity of the slopes of the reactive and nonreactive decay curves at longer lifetimes has been observed earlier for the ground-state reaction.[25] The fact that at a given E_{coll} at long lifetimes the slopes of the reactive and nonreactive lifetime distribution curves are almost the same means that the ratio of the probability of reactive to nonreactive decomposition remains

almost constant above 0.5 ps. No statistical complex would exhibit this kind of behavior, so the observation of stationary decay is another indication that neither of the two reactions is statistical. Furthermore, while in reaction R1 the number of nonreactive collisions exceeds that of the reactive ones by one or two orders of magnitude, in R2 at higher energies the decay curves almost coincide not only above 1 ps, but also starting from 0.3 ps (at low lifetimes, obviously, there are much more instantaneous nonreactive than reactive collisions). The coincidence means that if the complex lives long enough, the chance for decomposition into reactants and products is comparable. This is remarkable considering that the reactive collisions need not pass a barrier and exit at a much lower potential energy asymptote while those not reacting need to surmount the barrier they already passed on the way into the well. This latter scenario is obviously energetically less favorable. It is made to occur relatively frequently by the combination of the shape of the PES and the masses of the atoms, in particular, that it is the light H atom that can be bounced back from two heavy O atoms. This indicates that dynamics governs reaction R2 even in the relatively long lifetime range: the process does not follow the expectation based on energetics nor on a qualitative estimate of open channels corresponding to statistical theory (according to which the ratio of the two complex decomposition rates should depend on the total energy).

D. Hydrogen-atom transfer within the collision complex In the equilibrium geometry of HO_2, the H atom is connected to one of the O atoms. However, the potential energy surface is symmetric with respect to the interchange of the O atoms, so that there are two potential wells corresponding to HOO' and one to HO'O and they are separated by a potential barrier at a symmetric triangular geometry. The height of the barrier is well below the dissociation energy, which means that all HO_2 molecules formed by capture have much more energy than needed for isomerization. The occurrence of H-atom transfer from one O to the other has

been observed on both the ground- and the excited-state potential surfaces[25,39]. Detailed investigation of the isomerization proves to be fruitful in finding the reason for the high rotational and often vibrational excitation of the product OH radicals. For the analysis, we distinguish the following classes of trajectories. i) Captured or complex-forming trajectories (C). ii) "isomerization" trajectories, I, in which the H atom switches at least once from one O atom to the other; iii) 'L' trajectories: those 'I' trajectories in which the OH radical departs right after the last crossing of the isomerization barrier; iv) 'not L' means the complex oscillates for a long time after the last isomerization until it decomposes to O + OH; v) 'S' trajectories: those 'L' trajectories in which the O-O bond is in the stretching phase when the H atom leaves the barrier; vi) trajectories not undergoing isomerization at all (non-I). In addition, indices R and NR will distinguish quantities referring to reactive and nonreactive complex-forming trajectories. Table 1 shows the following ratios for both reactions R1 and R2: C(R)/(C(R)+C(NR)), the reactive fraction of complex-forming collisions, (I(R)+I(NR))/(C(R)+C(NR)), I(NR)/C(NR) and I(R)/C(R), the fraction of isomerizing trajectories out of all, out of the nonreactive and out of the reactive complex-forming ones, resp. (note that C(R) is in fact equal to the number of reactive collisions); I(R)/(I(R)+I(NR)), the fraction of reactive collisions out of all trajectories undergoing isomerization; L(R)/I(R), the fraction of 'L' trajectories out of the reactive isomerization trajectories and S(R)/L(R), the fraction of 'L' trajectories in which the O-O bond is in the stretching phase at decomposition. It is easy to see that the vast majority of reactive collisions involve isomerization for both reactions. In reaction R1, independently of the collision energy, about one third of the HO_2 complexes undergo isomerization, while in reaction R2 the 'I' fraction increases from about 20% at collision energies close to threshold to close to 50% at high collision energies. I(R)/C(R) shows that reactive events are intimately connected to isomerization: uniformly in about 90% of reactive collisions the H atom first makes a bond with one of the oxygens and switches to

the other. According to animation of such collisions, in the majority of such events, the H atom hops back and forth several times, often so that the OH initially formed rotates around its O atom and when the H approaches again the other O, the existing O–H bond breaks and a new one is formed. A difference between the two reactions is that in R1 only a few percent of trajectories involving isomerization will lead to reaction, increasing from 2% at threshold to a 7% at high E_{coll}: isomerization is close to being necessary but is far from being a sufficient condition for reaction. In R2, isomerization is more strongly tied to reaction: at low collision energy as high as 96% of all trajectories involving H-atom shift will react. This fraction decreases to below 40% at high E_{coll}, and an increasing part of complex-forming collisions involving isomerization will not lead to reaction. In other words, as the collision energy increases, isomerization becomes more frequent but it is less likely to "guarantee" reaction. The difference between reactions R1 and R2 can be again understood in terms of the potential surfaces. In R1 there is no barrier, the well is deep and the captured trajectories frequently undergo isomerization, even below the threshold for reaction. Even when there is enough energy, only a small fraction (1 to 3 %) of collisions lead to reaction, and this is reflected in the small probability that a collision involving isomerization leads to reaction. Note, however, that the probability of reaction is twice as large among 'I' trajectories than in all collisions. On the excited-state PES, on the other hand, as much as 20% of captured trajectories lead to reaction (note that for capture, the system needs to pass over the entrance barrier). At low collision energy the nonreactive collisions are mostly instantaneous and are reflected from the inner wall of the HO_2 potential well. Those trajectories that live long enough to explore the double potential well will very probably isomerize and also react. As the available energy increases, more trajectories undergo isomerization due to the high impact energy, but also because of the larger energy content, an increasing fraction of such collisions can get across the potential barrier back to reactants. Although this means that the

nonreactive fraction of the isomerization trajectories increases, virtually at the price of the reactive ones, the reaction probability in fact remains close to constant because the number of all isomerization trajectories increases.

The animations of trajectories indicated that very frequently, the reaction takes place right after the H atom, coming from one of the O atoms, rolls down on the isomerization barrier toward the other O ('L' trajectories). On the ground-state PES the fraction of such trajectories out of all isomerizing ones is 20 to 50%. In R2, the 'L' fraction is much larger, 60 to 80%. In addition, when the reaction takes place according to this scenario, in the overwhelming majority of cases (85 to 95%), the O–O vibration is in the stretching phase ('S' trajectories). When the H atom crosses the barrier and flies toward the potential well of one of the O atoms, its momentum carries it on the wall of the well which turns it toward the O and, if the O–O vibration is in the stretching phase, the well flattens and the H atom grabs the O with it. Because the two atoms meet at an angle with respect to the O–O bond, significant angular momentum arises. This is the ultimate reason for the remarkable rotational excitation of the product OH radical in both reactions, and accounts also for the often large vibrational excitation. The validity of this conjecture can be tested by comparing the outcome of reactive collisions in which no isomerization takes place (the 'non-I' class) or the H atom lingers around one of the O atoms for a long time after the last isomerization (the 'not-L' class). For both reactions at various initial quantum states and collision energies the slope of the lifetime distributions is very similar for the 'L' and 'non-I' classes of trajectories, but that of the 'not L' class is less steep, indicating that if a trajectory missed the chance of reaction right after isomerization, it will either become nonreactive or can form products only after a long intracomplex vibration. Remarkable difference can be seen between the translational and rotational distributions of the 'L' versus the 'not-L' and 'non-I' classes of collisions. As Fig. 7 shows, the 'L' collisions induce hotter translational distribution for both R1 and R2, while

in the other two classes much less translational energy is released. Shown in Fig. 8 are the vibrationally resolved rotational distributions of the OH products for reaction R2 (for R1 the differences can not be seen so clearly due to the noise in the data). The 'not-L' and 'non-I' classes behave similarly and differ from the 'L' class. While the width of the rotational distributions are similar, the major difference is that the 'L' class produces vibrationally less excited OH radicals than the other two. Overall, in the 'L' type collisions relatively more energy is channeled into translation and less to vibration than in 'not-L' and 'non-I' collisions. This supports the visual observation that in 'L' collisions, after the final isomerization step the OH radicals collect significant rotational excitation. They carry away the O atom relatively fast, which is due to the fact that for reaction it is favorable if the distance of the O atoms is increasing when the H atom arrives from the isomerization barrier.

E. Reaction stereodynamics Differential cross sections of products formation obtained for the reaction of both the ground- and excited-state O_2 shown in Fig. 9 display forward-backward symmetry in the center-of-mass coordinate system at low collision energies and low initial O_2 angular momentum, which is a signature of statistical behavior. This is in agreement with the exponential lifetime distributions of the complexes observed at low E_{coll}. At high collision energies dynamical effects are more significant: the forward peak increases concomitantly with the reduction of the complex lifetime. For the ground-state reaction, the forward-backward symmetry has been observed earlier[25] at as high collision energies as 130 kJ/mol, where the collision lifetime is far too short from being enough for the collision complex to perform several rotations that would ensure isotropic scattering. Based on animations, it was proposed that the forward-backward symmetry results from osculating complexes in which the encounter is short, but the direction of the products' relative velocity is more-or-less statistical because the O_2 molecule is randomly oriented at the beginning of the encounter. Another peculiarity is that when the initial angular momentum of O_2 increases,

the angular distribution flattens out both for reactions R1 and R2: the contribution of sideways scattering increases. This has also been seen for the reaction of triplet O_2 and was found[25] to be the most expressed at high collision energy. Similar phenomena can be observed in the case of nonreactive collisions that go through complex formation.

To understand the origin of this anisotropy in the scattering process we looked at detailed vector correlations. We calculated trajectories at three limiting orientations (see Fig. 10) of the angular momentum vector ***j*** of reactant O_2 with respect to the plane defined by the initial relative velocity vector (or the wave vector ***k***) and the initial orbital angular momentum ***l***: 1.) helicopter: plane of O_2 rotation parallel to the ***k-l*** plane, ***j*** perpendicular to both ***k*** and ***l***, H atom approaches out of the O_2 rotation plane; 2.) propeller: plane of O_2 rotation perpendicular to the ***k-l*** plane; ***j*** parallel to ***k***; 3.) cartwheel: plane of O_2 rotation perpendicular to the ***k-l*** plane, ***j*** parallel to ***l*** (direction of approach of H in the O_2 rotation plane). 200,000 trajectories were calculated at several collision energies at fixed ***j***, ***k***, ***l*** arrangements corresponding to each of the limiting cases described above. The vibrational quantum number of O_2, the magnitude of ***j*** as well as E_{coll} were set to fixed values. The remaining parameters, including the impact parameter, the phase of vibration of the oxygen molecule, the sign of its angular momentum and the initial rotational angle of O_2 were selected by Monte Carlo sampling. In a set of calculations, the impact parameter was also fixed.

As shown in Fig. 11, the helicopter and cartwheel arrangements yield forward-backward symmetric angular distributions for both reactions R1 and R2; the patterns obtained on the two PES are remarkably identical. Sideways scattering can only be observed for the propeller set-up, but even then only when the O_2 is initially rotationally excited. This means that the O_2 molecule has to rotate to induce sideways scattering. Taking this into account, the behavior of the propeller set-up is not surprising: in this arrangement the velocity vector of the oxygen atoms is always perpendicular to the direction of attack. When the O–O bond breaks, the O

atoms keep their direction of momentum, one of them carrying the light H atom. Because the sideways scattering is important in the overall angular distributions (Fig. 9), one can conclude that the propeller-type collision arrangement contributes significantly to the reactive cross section, at least when the O_2 is rotationally excited.

Interestingly, sideways scattering is observed for both reactions R1 and R2, even though in the entrance channel the R1 potential surface is purely attractive while on the R2 PES the entrance to the potential well is blocked by a potential barrier. One can surmise that a common factor is responsible for the identical dynamics of the two reactions. What is common in reactions R1 and R2 is that i) the mass combination of atoms is the same: a light H atom attacks a molecule consisting of two heavy O atoms and ii) the location of the entrance to the potential well on the PES is similar. The PES effect in more detail: for reaction R1, the potential energy monotonically decreases if the H atom approaches the OO' molecule in the H–O–O' angle range of roughly 150° to 165°. Because the two atoms are identical, the potential is also attractive in the same range of the H–O'–O angle. Both ranges represent the entrance to the HOO' potential well, and, since the O_2 molecule can be approached at any (polar) angle around its axis, the spherical angle range where the approaching H atom is attracted forms two spherical bands around the O-O' axis schematically shown in Fig. 12 similar to those between the Tropic of Cancer and the Arctic Circle and between the Tropic of Capricorn and the Antarctic Circle on Earth. For reaction R2, although the potential through the entrance to the well is not monotonically decreasing, the HO_2 well is accessible from spherical angles that are essentially the same as on the PES of reaction R1. We shall refer to these spherical domains as “bands of acceptance”.

The effect of the mass combination and the role of the bands of acceptance is manifested in different dynamical observables. For the forward-backward symmetry of the angular distributions in the cartwheel and helicopter arrangements and the sideways peak in the

propeller set-up obviously the mass effect is responsible. Really, if one sets the mass of the H atom to 16 $gmol^{-1}$, the sideways peak washes out. (Note that the forming O–^{16}H molecule will still heavily rotate, but the position of the angular momentum peak is shifted to a value that is a factor of 4 larger than for regular OH.)

The signature of the "bands of acceptance" can be expected to appear in the opacity functions: it is tempting to expect that if the reactivity is large at impact parameters where the H atom hits one of the bands of acceptance, then the dynamics is governed by the chance of entering the HO_2 well. Fig. 13 shows the opacity functions for reaction and for complex formation in the three arrangements at a collision energy of 96.5 kJ/mol for both R1 and R2. Again, the propeller arrangement differs from the other two, in the same way for both reactions. The role of entering the potential well can be extracted from Fig. 13b, which shows the opacity function for nonreactive complex-forming collisions. The probability of entering the potential well at different impact parameters is well characterized by that of nonreactive complex-forming events, because the majority of collisions in which a complex is formed according to the definition presented in the Methods section, are nonreactive, The probability of complex formation for both reactions in the cartwheel and helicopter arrangements is large at small impact parameters and when *b* is increased, decreases (for the helicopter arrangement, after passing a flat maximum near *b*=0.5 Å). This differs from the shape of the reactive opacity function, which passes a well-defined maximum. Completely different is the opacity function for complex formation in the propeller set-up: it increases in the *b*=0 to 0.5Å range from zero to a limiting high value where it stays large until falling down at around *b*=2 Å as quickly as it rose. The difference between the dynamics in the cartwheel and helicopter arrangements versus the propeller set-up can be understood by looking at Fig. 10. When the O_2 molecule rotates, the axis of rotation is a perpendicular bisector of the O–O bond (can be selected to be the X axis in the coordinate system shown in the figure) or if it does not rotate,

the angle between the O-O axis and the plane of the plot (the X-Y plane) is random. This means that the bands of acceptance can point in any direction, making possible for the H atom to hit it at any impact parameter within about 2 Å. Imagining a situation in which the O_2 molecule rotates about the X axis, the cartwheel arrangement corresponds to the attack by the H atom in the Y-Z plane, along a path parallel to the Z axis (which is perpendicular to the plane of the plot) in Fig. 10, at impact parameters measured along the Y axis. At any impact parameter below about 2 Å, the H atom can find a number of molecules whose bands of acceptance happen to be turned to meet the line of attack. Similar is the helicopter case where the attack is parallel to the Z axis in a plane that is parallel to the Y–Z plane and is displaced along the horizontal axis by the impact parameter. In both cases, the band of acceptance is most probably hit at small impact parameters, from which the opacity function decreases. In the propeller arrangement, the approach is in the plane of the plot, the line of attack being parallel to the horizontal (X) axis. b=0 means that the H atom attacks at the center of mass of O_2, from where it is repelled by the repulsive wall, with no chance of complex formation. With increasing b, the line of attack is gradually shifted up (or down) in Fig. 10) into the band of acceptance whose center is at around 1 Å. The H atom is allowed into the well up to about b=2 Å. (The band of acceptance is in fact somewhat widened by the O–O vibration.) This rationalizes the arrangement dependence of the opacity function for complex formation.

The shape of the opacity functions for reaction is completely different. In the helicopter and cartwheel set-up the reaction probability is significant at zero impact parameter. For reaction R2 it increases with the increase of b until it passes a maximum near b=1 Å while in reaction R1 the reaction probability remains large until about 1.5 Å where it starts to decrease relatively fast; the maximum is not well expressed. In the propeller set-up the opacity function is drastically different: the reaction probability is zero at b=0 and shows two maxima at about b=0.3 and 2 Å for reaction R1, and at b=0.5 and 1.75 Å for reaction R2. However,

the shape of the opacity function for reaction in any of the three arrangements is very much different from that of complex formation which characterizes the chance of entering of the potential well, The large difference indicates that out of the complexes formed, those in which the H atom enters the potential well at certain impact parameter ranges are more probable to react. This is another signature of the enhanced role of dynamics in these reactions: the complexes formed retain the memory of the way they were formed. We found it instructive to analyze the reactivity pattern in the three set-ups. The maxima of the reactive opacity functions at about b = 1 Å in the helicopter arrangement (spectacularly sharp on the R2 PES) can be rationalized by viewing Fig. 10 again: when the H atom attacks in this impact parameter range, it goes from sideways into the HO_2 potential well. For example, when the O_2 happens to be perpendicular to the plane of the plot, the H atom will fly parallel to the O–O axis. After it makes the first O–H bond with the O atom closer to it, its momentum can easily make it switch to the farther O atom. As it was shown in section D, this kind of isomerization is favorable for reaction. In the propeller arrangement, the direction of attack is always perpendicular to the O–O bond. When the impact parameter is small (about 0.5 Å) or large (say 2 Å) the H atom enters the well at a bent arrangement. At small impact parameters (shown schematically in Fig. 14, black line) its path is deflected by the repulsion at the center of the O–O bond and is directed towards the outer repulsive wall of the well. According to animation of this kind of trajectories, the H atom is generally reflected towards the isomerization barrier, leading to a switch from the HO'O to the O'OH arrangement. Such collisions are often prompt. When the H atom approaches at a large impact parameter (Fig. 14, orange line) the H atom is directed towards the center of the O-O bond by the repulsive potential centered along the O–O axis. The H atom hits the wall around the core of the O atom, from where it is reflected into the inner repulsive wall and back, which in many collisions is repeated several times, and the exit generally is an isomerization. The lifetime of

this kind of complexes is much longer than that of the small impact-parameter encounters. Since isomerization is advantageous for reaction, at impact parameters where its chance is larger the reaction probability will be larger than elsewhere, which explains the peaks at around 0.5 and above 2 Å. When the H atom enters the potential well near b=1 Å, almost at the equilibrium geometry of the HO_2 complex, it generally hits the repulsive wall almost perpendicularly. Even when it is not reflected promptly, the bend excitation will be less expressed, making the conditions for isomerization less favorable, inducing the dip on the opacity functions in the propeller arrangement.

CONCLUSIONS

The H + $O_2(^1\Sigma_g)$ (R1) and H + $O_2(^1\Delta_g)$ (R2) pair of reactions allow one to make comparisons and assign dynamical observables to various features of the potential energy surfaces of this kind of complex-forming bimolecular reactions. What is common in the two reactions is that an HO_2 complex is formed before O and OH are produced. The potential well is separated by an isomerization barrier into two corresponding to the H atom being connected to one or the other O atom. This barrier is way below the reactant energy level in both cases. The major differences are that reaction R1 is endothermic, without any barrier in the entrance or exit regions, while R2 is exothermic and has a relatively low barrier in the entrance channel. These features suggest that the reaction can formally be separated into two phases: complex formation and complex decomposition into products (and unavoidably, back to reactants). These differences are manifested in the influence of rotational excitation of O_2 on rate of the two reactions. The O_2 rotation spectacularly enhances the reactivity in R1, not by facilitating complex formation but by providing energy for climbing out of the potential well on the product side after intramolecular energy exchange. In contrast, in the exothermic R2 reaction, rotational excitation of O_2 is hardly effective in inducing reaction, because it can only slightly

increase the chance of getting across the potential barrier. The extra energy can not have a significant influence of the probability of the decomposition of the complex simply because it is not needed: once the system passes the entrance barrier, it has plenty of energy to get out of the potential well on the O+OH side. Common in the two reactions is that the product OH molecules are rotationally hot, and in reaction R2 they also carry significant vibrational energy. The presence of the isomerization barrier proved to be instrumental in explaining this common feature. In a large fraction of collisions the H atom, after building a bond with one of the O atoms, switches to the other, and the isomerization can be repeated many times. The majority of reactive collisions involve at least one such switch. Sliding off the isomerization barrier proves to be favorable for reaction: the H atom moves at a small angle to the O–O bond, and is attracted toward the O atom. Its momentum keeps it moving on a curved path when it can grab the O atom, favorably in the stretching phase of the O–O vibration, thus resulting in fast rotation (and often translation) of the product. The fact that the H atom is much lighter than the O atoms is a major factor facilitating this mechanism. Nonreactive collisions also display a signature of the properties of the PES. In those collisions in which the H atom hits the outer repulsive wall of the PES, it is reflected with minor translation–to–rotation energy transfer. In contrast, when the H atom is able to enter the potential well where the interactions are strong, very large T to V,R energy transfer can be observed, similarly to the frustrated reactive encounters seen in the H + vibrationally excited water reaction[53]. The highly inelastic collisions generally do not require a long time in the potential well for energy exchange; instead, most of them is impulsive: the H atom enters the well, hits the inner repulsive wall of the potential well and departs, carrying a large amount of vibrational energy.

The disc shape of the rotating O_2 molecule also induces a common feature for the two reactions. The product OH radical is significantly sideways scattered with respect to the

forward-backward symmetric distribution expected for a long-lived complex. This phenomenon is enhanced when the O_2 molecule is initially rotationally excited. The extra sideways scattering has been found to originate in collisions with a propeller-like arrangement, and can not be explained by angular momentum effects expected for a light + heavy-heavy mass combination. The collisions in this special arrangement also shed light to the mechanism of the reaction. In both reactions, the opacity function for complex formation follows the expectations, while that for reaction is completely independent of the former, indicating that the intramolecular dynamics is common for the two reactions, once the system has entered the potential well.

The authors declare no competing financial interest.

ACKNOWLEDGMENT

We are grateful to Professors Hua Guo and Daiquin Xie for providing us with the potential energy surface code. This work was supported in part by the Hungarian Scientific Research Fund (Grant No. OTKA K108996) and by the National Development Agency (Grant No. KTIA_AIK_12-1-2012-0014 and TÁMOP-4.2.2.A-11/1/KONV-2012-0064).

APPENDIX

The original XXZLG[45] and LXDJMG[37] PES codes use a spline fit with the O–O' distance, one of the H–O distances, r(H–O), and the H–O–O' angle as coordinates. Only one half of the fitted PES; which we call the left-hand side, LHS part, V_{LHS} is used. This part corresponds to geometries from the collinear H–O–O' arrangement to the C_{2v} geometries where the two H-O distances are equal. In this region (H–O–O' type geometries), r(H–O) is always smaller than r(H–O'). In the region where r(H–O) > r(H–O'), which we shall call right-hand side (RHS) part (O–O'–H geometries) the potential energy V_{RHS} on the full spline-fitted PES is different from that at its symmetric H–O–O' counterpart. The PES (denoted as V_{orig}) was made

symmetric by calculating the potential energy for RHS geometries by the authors of the two PES codes using r(H–O') instead of r(H–O) and changing the angle to H–O'–O, which is equivalent to using the LHS PES for LHS geometries and its mirror image for RHS geometries:

$$V_{orig}(r(\text{O–O}'), r(\text{H–O}), r(\text{H–O}')) = \begin{cases} V_{LHS}(r(\text{O–O}'), r(\text{H–O}), r(\text{H–O}')) & \text{if } r(\text{H-O}) \le r(\text{H-O}') \\ V_{LHS}(r(\text{O–O}'), r(\text{H–O}'), r(\text{H–O})) & \text{if } r(\text{H-O}) > r(\text{H-O}') \end{cases} \quad \text{(A1)}$$

However, since the spline fit does not reflect the symmetry of the PES, the energy does not change smoothly at C_{2v} geometries (among them the isomerization barrier): the LHS part and its mirror image cross each other at a seam along the C_{2v} symmetry plane. As a consequence, the gradient is discontinuous, which under some conditions destroys energy conservation when a trajectory crosses the seam.

To remove this singularity and still preserve the symmetry of the PES, we designed a switching procedure that guarantees that the modified LHS and RHS parts meet so that at the C_{2v} arrangement the derivative of the PES along lines perpendicular to the C_{2v} symmetry plane is zero, moreover, the energy at the crossing seam remains the same as the LHS part of the PES dictates. The procedure is as follows: We use the original setup of the code (LHS energies at LHS geometries and the mirrored LHS energies at RHS geometries) only when the H atom is far (see below) from the T-shaped arrangement. At every call to the potential energy subroutine we test whether the system is close to the C_{2v} geometry by calculating the difference between the H–O and H–O' distances. When the absolute value of the difference, $r_{\text{diff}} = |r(\text{H–O}) - r(\text{H–O}')|$ decreases below 0.1 Å, we switch from the original symmetrized PES denoted as V_{orig} to the average of the LHS part and the mirror image of the RHS part of the *unsymmetrized* XXZLG or LXDJMG PES, V_{avg},

$$\begin{aligned} &V_{avg}(r(\text{O–O}'), r(\text{H–O}), r(\text{H–O}')) \\ &= \left(V_{LHS}(r(\text{O–O}'), r(\text{H–O}), r(\text{H–O}')) + V_{RHS}(r(\text{O–O}'), r(\text{H–O}), r(\text{H–O}'))\right)/2 . \end{aligned} \quad \text{(A2)}$$

The switching is made the same way, symmetrically on both sides of the C_{2v} geometry:

$$V_{smooth} = S\ (x)V_{orig} + (1 - S(x))V_{avg} \tag{A3}$$

where $x = 10r_{diff}$, *i.e.*, the switching function decreases from unity at r(H–O)–r(H–O')=0.1 Å to zero at r(H–O) = r(H–O') and then increases to unity by r(H–O)–r(H–O')= –0.1 Å. We applied the switching function designed by Johnson[54] which guarantees that in the $0 < r_{\mathrm{diff}} <$ 0.1 Å region the switch is smooth and continuously differentiable up to the fourth order.

$$S(x)=\begin{cases} 0 & x\le 0 \\ -x^4\left(\left((20x-70)x+84\right)x-35\right) & 0<x<1 \\ 1 & 1\le x \end{cases} \tag{A4}$$

Figure A1 shows the V_{orig} (V_{LHS}), the V_{RHS} and the V_{avg} potential curves together with the smoothed one in the switching region when r(O–O')=1.2 Å.

TABLES

Table 1

Ratios characterizing complex formation for reactions R1 and R2 at four selected collision energies

$O_2(^3\Sigma^-_g)$ $v = 0$, $j = 1$	E_{coll} / kJ/mol			
	57.9	**62.7**	**77.2**	**96.5**
C(R)/(C(R)+C(NR))	0.01	0.01	0.02	0.03
(I(R)+ I(NR))/(C(R)+C(NR))	0.37	0.36	0.35	0.36
I(NR)/C(NR)	0.36	0.35	0.34	0.35
I(R)/C(R)	0.90	0.88	0.85	0.81
I(R)/(I(R)+I(NR))	0.02	0.02	0.05	0.07
L(R)/I(R)	0.21	0.25	0.33	0.48
S(R)/L(R)	0.93	0.93	0.95	0.95

$O_2(^1\Delta_g)$ $v = 0$, $j = 0$	E_{coll} / kJ/mol			
	33.8	**48.2**	**67.5**	**96.5**
C(R)/(C(R)+C(NR))	0.20	0.20	0.20	0.18
(I(R)+ I(NR))/(C(R)+C(NR))	0.19	0.24	0.36	0.44
I(NR)/C(NR)	0.01	0.08	0.22	0.33
I(R)/C(R)	0.87	0.91	0.93	0.91
I(R)/(I(R)+I(NR))	0.96	0.74	0.52	0.38
L(R)/ I(R)	0.61	0.65	0.71	0.79
S(R)/ L(R)	0.89	0.85	0.85	0.88

FIGURE CAPTIONS

Figure 1
The schematic representation of the potential energy surfaces for reactions R1 and R2. Energies in kJ/mol. *i* denotes the isomerization barrier

Figure 2
Excitation functions for reaction R1 (closed symbols) and R2 (open symbols) for three different rotational states of the reactant O_2 molecule.

Figure 3
The effect of rotational excitation of O_2 on the probabilities of complex formation, of reaction and of nonreactive complex formation events for reactions a) R1 and b) R2. The O_2 is in vibrational ground state; the initial collision energies considered are 77.2 kJ/mol for reaction R1 and 33.8 and 96.5 kJ/mol for reaction R2. Note that in reaction R1 the reactive reaction probabilities are two orders of magnitude smaller than those of complex formation, and the latter are essentially the same as those of complex-formation not resulting in reaction.

Figure 4.
Vibrationally resolved product rotational distributions for reaction R1 and R2 at a collision energy 96.5 kJ/mol. The O_2 reactant is in vib-rotational ground state.

Figure 5.
Vibrational distribution of O_2 after nonreactive complex-forming collisions in reactions R1 (a) and R2 (b).

Figure 6.
Lifetime distributions for reactive (closed symbols) and nonreactive complex-forming (open symbols) for reactions a) R1 and b) R2 at two collision energies.

Figure 7.
Product translational distributions for reactions R1 and R2 in collisions involving isomerization (I), in those in which the complex decomposes to O+OH right after isomerization (L) or significantly later (not-L), and in those where no isomerization occurs.

Figure 8.
Vibrationally resolved product rotational distributions in various classes of collisions for reaction R2. For notation see Fig. 7 and the text.

Figure 9
Product angular distributions for reactions R1 (a) and R2 (b) at three collision energies and at three different initial rotational excitations of the O_2 molecule

Figure 10

The helicopter, propeller and cartwheel arrangements used in the study of stereodynamics of reactions R1 and R2. $\boldsymbol{j}$ is the angular momentum of O_2; $\boldsymbol{l}$ is the orbital angular momentum. $\boldsymbol{k}$ is the wave vector roughly proportional to the momentum of the H atom and shows the direction of attack. *b* indicates the impact parameter, measured from the line of approach of

the H atom. The ***j*** vector is parallel to ***k*** in the propeller set-up and perpendicular to it in the other two. In the helicopter set-up the H atom attacks parallel to but out of the plane of O_2 rotation (except at zero impact parameter), in the cartwheel arrangement the attack is in the plane of rotation, while in the propeller set-up it is perpendicular to the plane of rotation of O_2.

Figure 11
Angular distributions at fixed orientations of the initial O_2 angular momentum ***j*** with respect to the ***k,l*** plane for reactions a) R1 and b) R2 at a medium collision energy

Figure 12
Sections of the potential energy surfaces for reactions R1 (left two panels) and R2 (right two panels) in the H–O–O plane as a function of the location of the H atom with respect to the center of mass of O_2 at the respective equilibrium O–O distance (top panels) and at r(O–O)=1.3 Å, the outer turning point in the second vibrational state of O_2 (bottom panels). O_2 is aligned along the y axis. The unit of energy is kJ/mol and is measured from those at the H + O_2 reactant limits with O_2 at its triplet (left panels) and singlet (right panels) equilibrium geometry. The small plot in the top right corner schematically indicates the bands of acceptance (see text). The Y axis is the molecular axis, the X axis is its bisector lying in the plane of the plot, the Z axis is perpendicular to the plane of the plot.

Figure 13
Opacity functions for reaction (a) and nonreactive complex formation (b) in reactions R1 and R2 in the limiting arrangements shown in Fig. 10.

Figure 14.
Schematic representation of the change of the mechanism with impact parameter in both reactions R1 and R2 in the propeller arrangement. The black line shows the typical path of the H atom in small impact parameter collisions, the red line that in large impact parameter collisions. The PES is shown in the same set-up as in Fig. 12.

Fig. A1.
The smooth switching of the PES of reaction R2 as a function of the difference between the two H–O distances at r(O–O')=1.2 Å.

Figure 1
The schematic representation of the potential energy surfaces for reactions R1 and R2. Energies in kJ/mol. *i* denotes the isomerization barrier

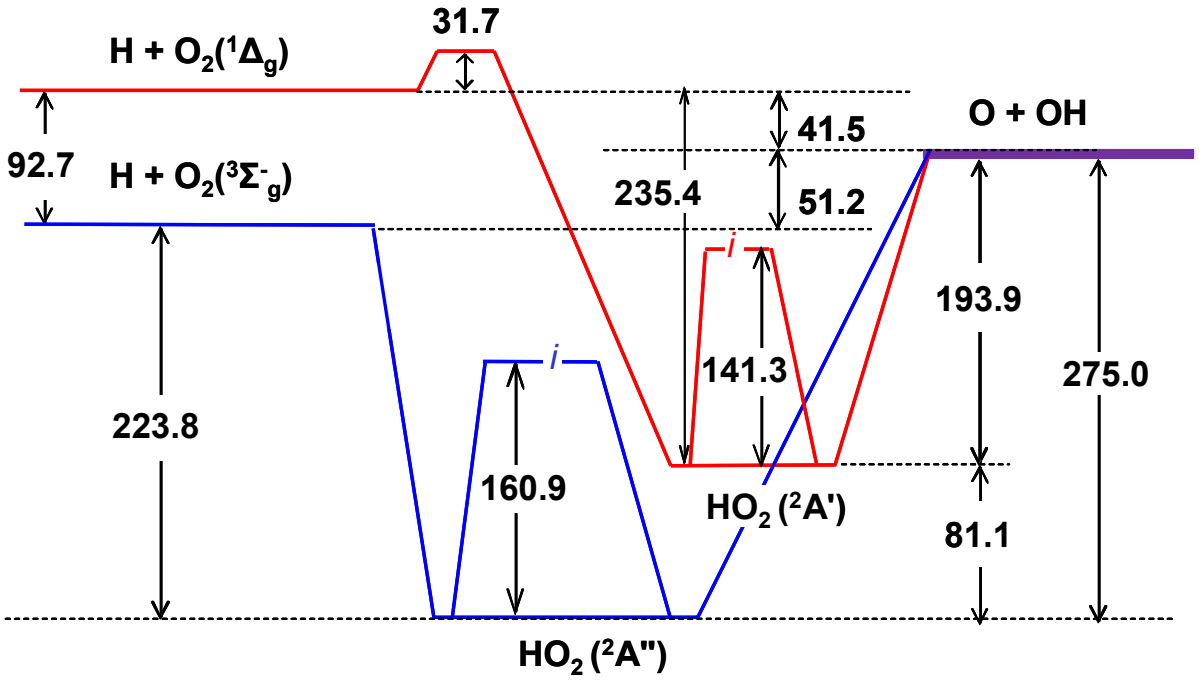

Figure 2
Excitation functions for reaction R1 (closed symbols) and R2 (open symbols) for three different rotational states of the reactant O_2 molecule.

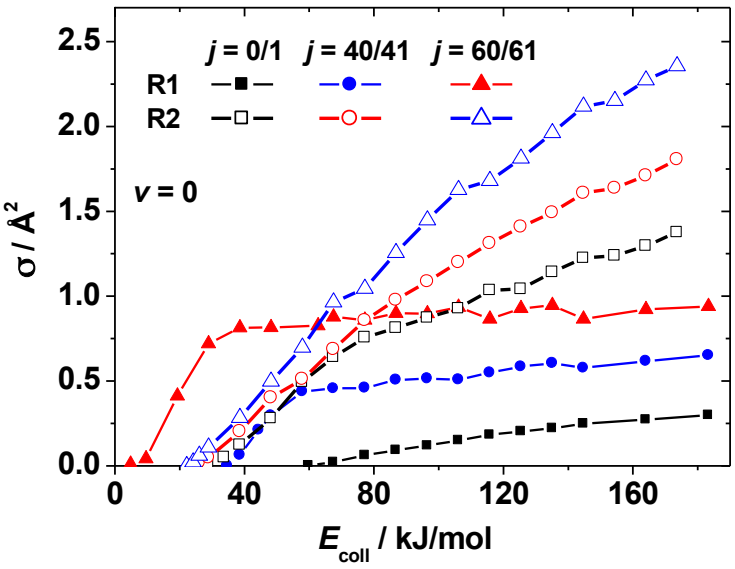

Figure 3
The effect of rotational excitation of O_2 on the probabilities of complex formation, of reaction and of nonreactive complex formation events for reactions a) R1 and b) R2. The O_2 is in vibrational ground state; the initial collision energies considered are 77.2 kJ/mol for reaction R1 and 33.8 and 96.5 kJ/mol for reaction R2. Note that in reaction R1 the reactive reaction probabilities are two orders of magnitude smaller than those of complex formation, and the latter are essentially the same as those of complex-formation not resulting in reaction.

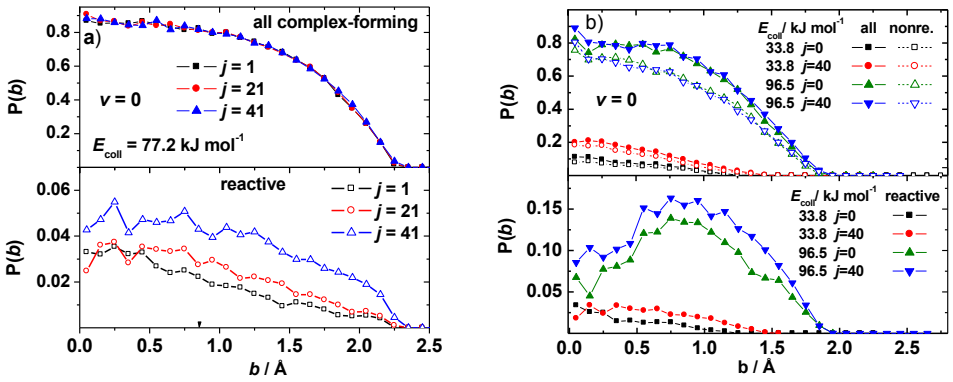

Figure 4.
Vibrationally resolved product rotational distributions for reaction R1 and R2 at a collision energy 96.5 kJ/mol. The O_2 reactant is in vib-rotational ground state.

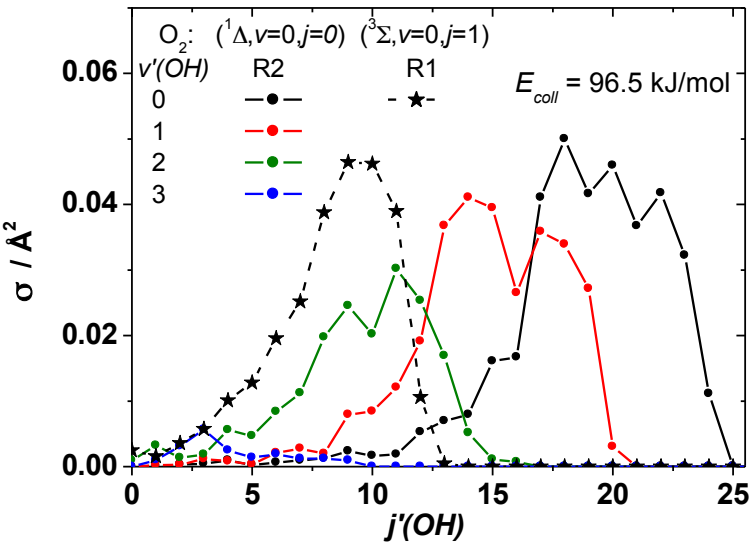

Figure 5.
Vibrational distribution of O_2 after nonreactive complex-forming collisions in reactions R1 (a) and R2 (b).

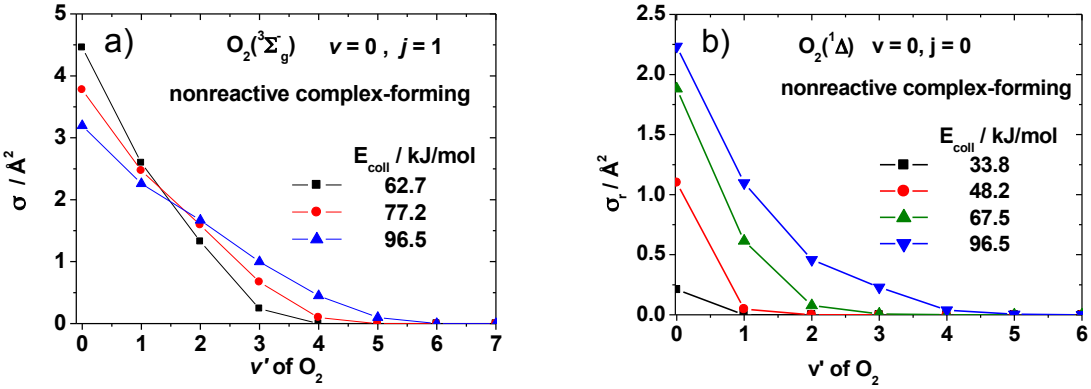

Figure 6.
Lifetime distributions for reactive (closed symbols) and nonreactive complex-forming (open symbols) for reactions a) R1 and b) R2 at two collision energies.

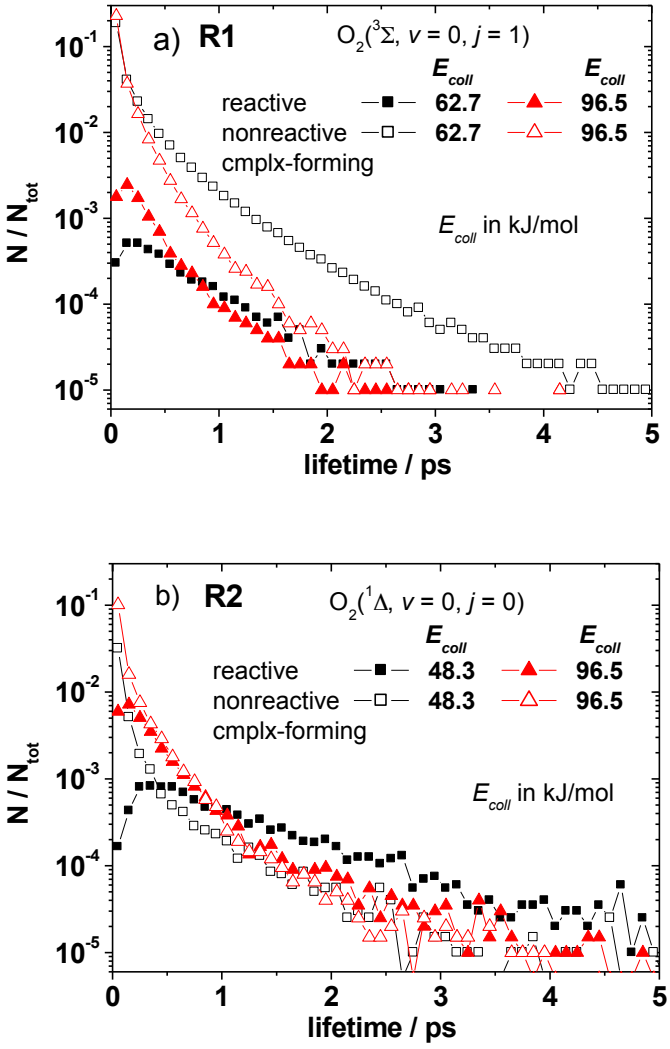

Figure 7.

Product translational distributions for reactions R1 and R2 in collisions involving isomerization (I), in those in which the complex decomposes to O+OH right after isomerization (L) or significantly later (not-L), and in those where no isomerization occurs.

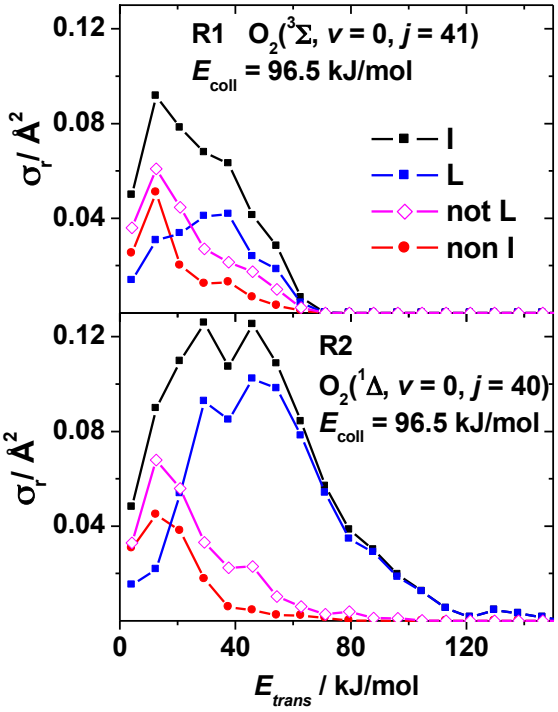

Figure 8.

Vibrationally resolved product rotational distributions in various classes of collisions for reaction R2. For notation see Fig. 7 and the text.

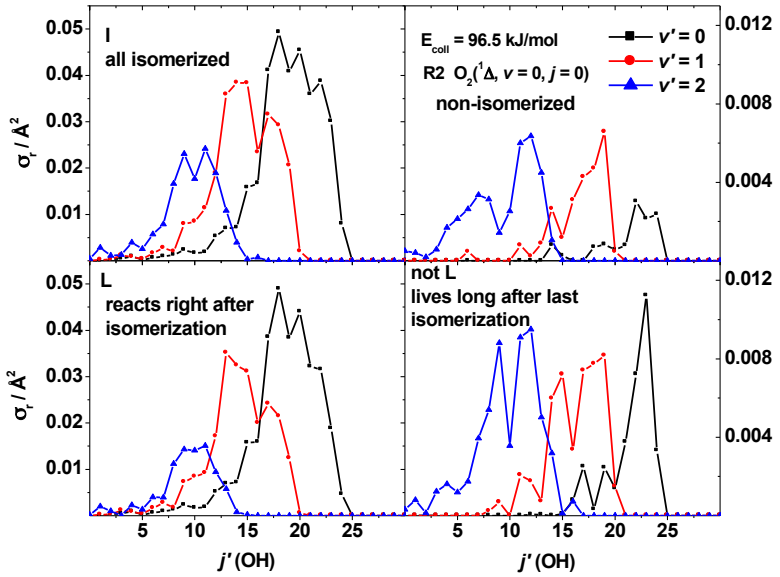

Figure 9
Product angular distributions for reactions R1 (a) and R2 (b) at three collision energies and at three different initial rotational excitations of the O_2 molecule

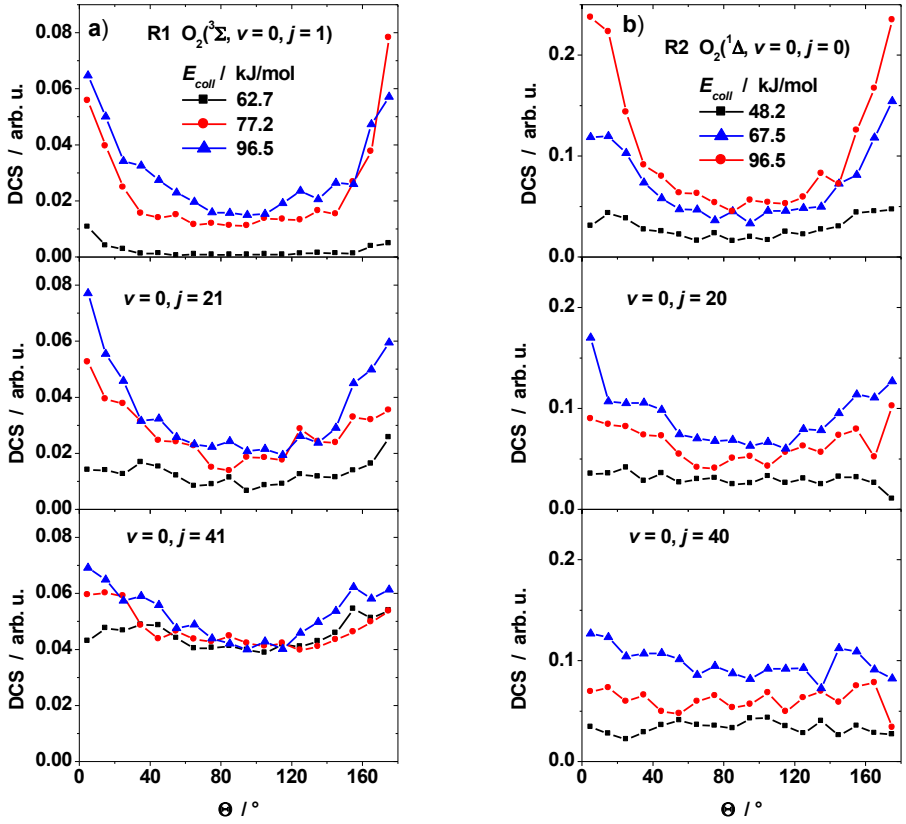

Figure 10

The helicopter, propeller and cartwheel arrangements used in the study of stereodynamics of reactions R1 and R2. ***j*** is the angular momentum of O_2; ***l*** is the orbital angular momentum. ***k*** is the wave vector roughly proportional to the momentum of the H atom and shows the direction of attack. *b* indicates the impact parameter, measured from the line of approach of the H atom. The ***j*** vector is parallel to ***k*** in the propeller set-up and perpendicular to it in the other two. In the helicopter set-up the H atom attacks parallel to but out of the plane of O_2 rotation (except at zero impact parameter), in the cartwheel arrangement the attack is in the plane of rotation, while in the propeller set-up it is perpendicular to the plane of rotation of O_2.

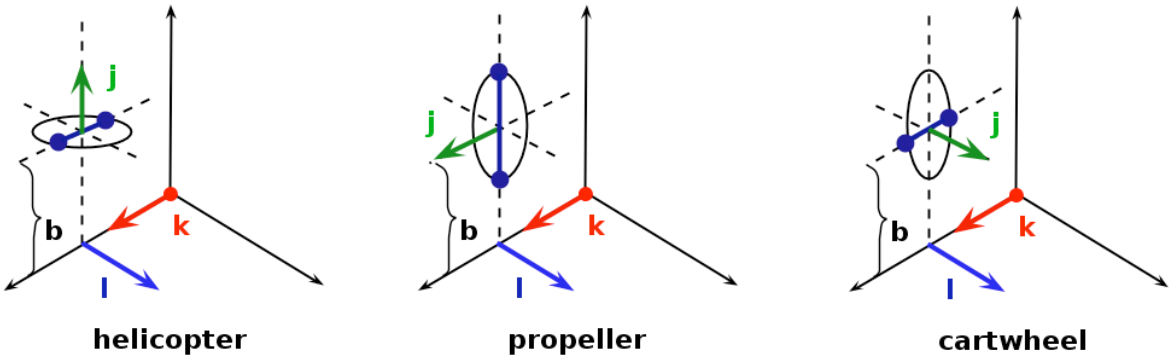

Figure 11
Angular distributions at fixed orientations of the initial O_2 angular momentum ***j*** with respect to the ***k,l*** plane for reactions a) R1 and b) R2 at a medium collision energy

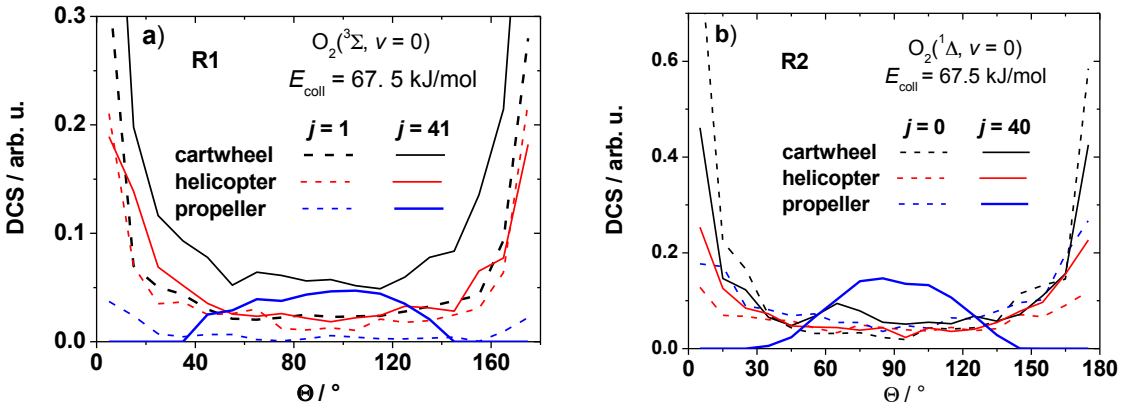

Figure 12
Sections of the potential energy surfaces for reactions R1 (left two panels) and R2 (right two panels) in the H–O–O plane as a function of the location of the H atom with respect to the center of mass of O_2 at the respective equilibrium O–O distance (top panels) and at r(O–O)=1.3 Å, the outer turning point in the second vibrational state of O_2 (bottom panels). O_2 is aligned along the y axis. The unit of energy is kJ/mol and is measured from those at the H + O_2 reactant limits with O_2 at its triplet (left panels) and singlet (right panels) equilibrium geometry. The small plot in the top right corner schematically indicates the bands of acceptance (see text). The Y axis is the molecular axis, the X axis is its bisector lying in the plane of the plot, the Z axis is perpendicular to the plane of the plot.

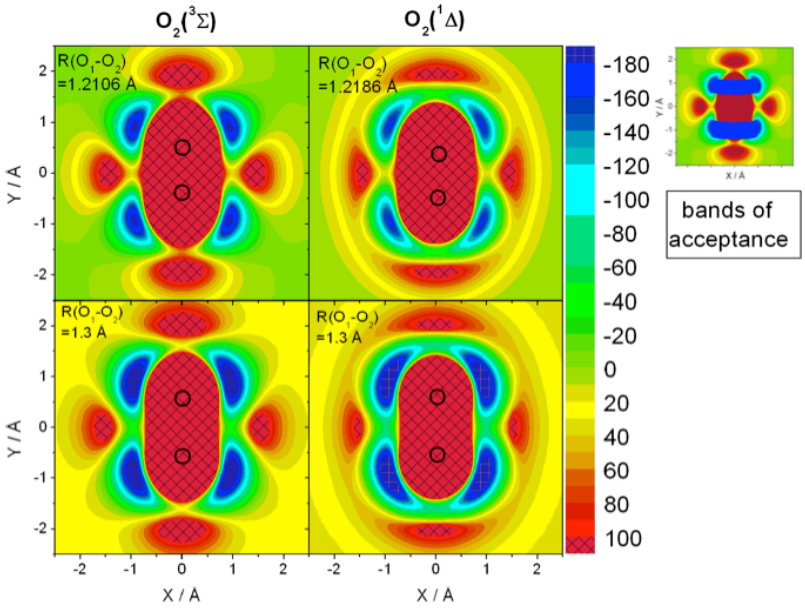

Figure 13
Opacity functions for reaction (a) and nonreactive complex formation (b) in reactions R1 and R2 in the limiting arrangements shown in Fig. 10.

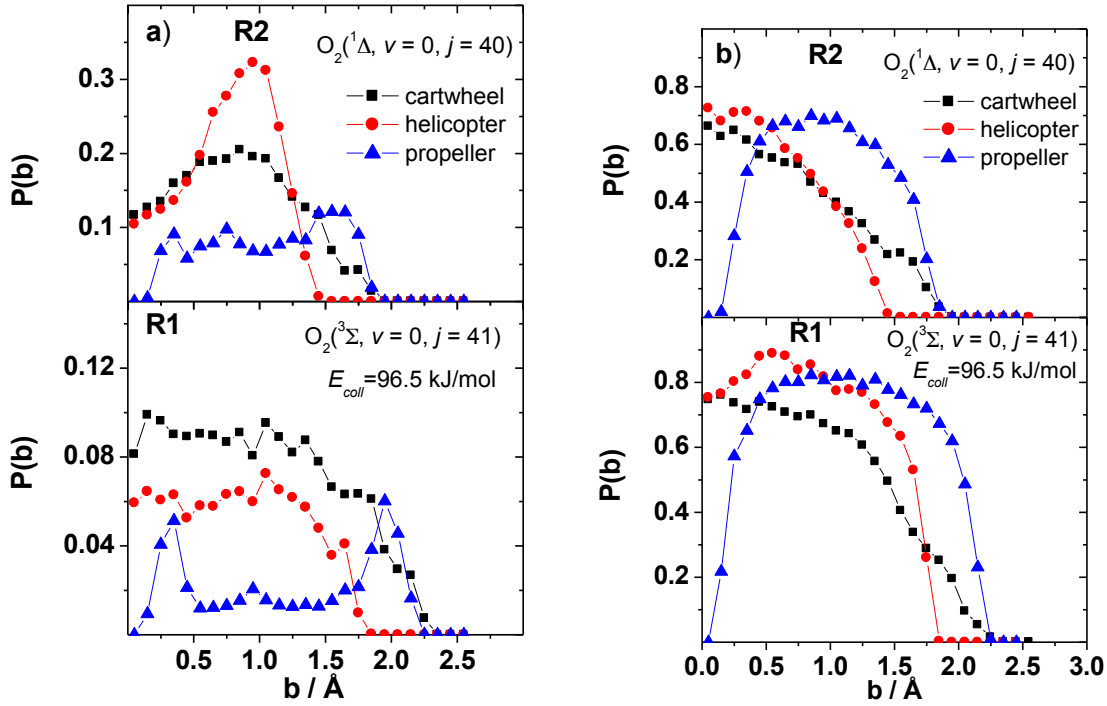

Figure 14.
Schematic representation of the change of the mechanism with impact parameter in both reactions R1 and R2 in the propeller arrangement. The black line shows the typical path of the H atom in small impact parameter collisions, the red line that in large impact parameter collisions. The PES is shown in the same set-up as in Fig. 12.

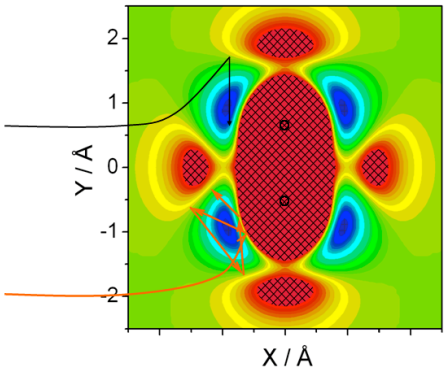

Fig. A1.
The smooth switching of the PES of reaction R2 as a function of the difference between the two H–O distances at *r*(O–O')=1.2 Å.

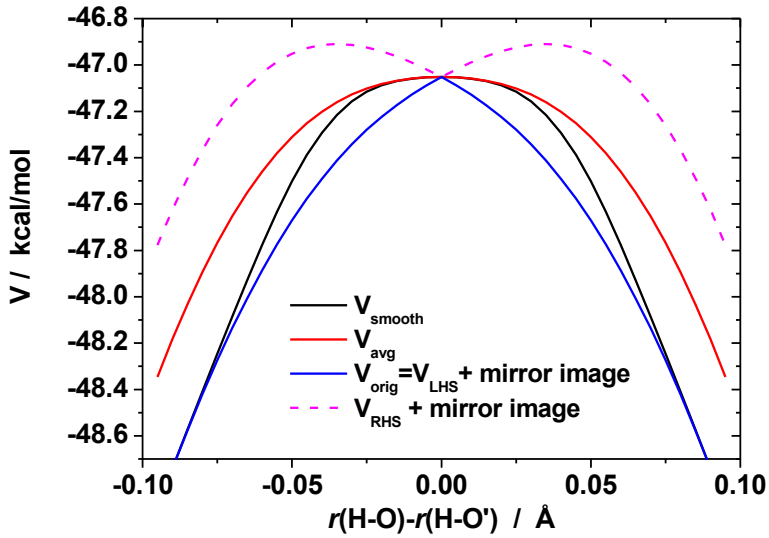

REFERENCES

[1] Eyring H.; Polanyi, M., Über einfache Gasreaktionen *Z. Phys. Chem., Abt. B*, **1931**, *12*, 279-311. In English: On Simple Gas Reactions, *Z. Phys. Chem.* **2013**, *227*, 1221–1245.

[2] Evans M. G.; Polanyi M., Notes on the Luminescence of Sodium Vapour in Highly Dilute Flames, *Trans. Faraday Soc.* **1939**, *35*, 178-185.

[3] Stark, K.; Werner, J., An Accurate Multireference Configuration Interaction Calculation of the Potential Energy Surface for the F+H_2 -> HF+H reaction, *J. Chem. Phys.* **1996**, *104*, 6515-6530.

[4] Welsh R.; Manthe U., Loss of Memory in H + CH_4 □ H_2 + CH_3 State-to-State Reactive Scattering, *J. Phys. Chem. Lett.*, **2015**, *6*, 338–342.

[5]Miller, J. A.; Kee, R. J.; Westbrook, C. K. Chemical Kinetics and Combustion Modeling, *Annu. Rev. Phys. Chem.* **1990**, *41*, 345-387.

[6]Miller, J. A.; Pilling, J. A.; Troe, J. Unraveling Combustion Mechanisms through a Quantitative Understanding of Elementary Reactions. *Proc. Combust. Inst.* **2005**, *30*, 43-88.

[7]Baulch, D. L.; Drysdale, D. D.; Horne, D. G.; Lloyd, A.C. Evaluated Kinetic Data for High Temperature Reactions, Vol. 1, Homogeneous Gas Phase Reactions of the H_2-O_2 System Butterworths, London, **1972**.

[8]Frank, P.; Just Th. High Temperature Reaction Rate for H + O_2 = OH + O and OH + H_2 = H_2O + H. *Ber. Bunsenges. Phys. Chem.* **1985**, *89*, 181-187.

[9]Pirraglia, A. N.; Michael, J. V.; Sutherland, J. W.; Klemm, R. B. A Flash Photolysis-Shock Tube Kinetic Study of the Hydrogen Atom Reaction with Oxygen: H + O_2-> OH + O (962 K

≤ T ≤ 1705 K) and H + O_2 + Ar → HO_2 + Ar (746 K ≤ T ≤ 987 K). *J. Phys. Chem.* **1989**, *93*, 282–291.

[10]Masten, D. A.; Hanson, R. K.; Bowman, C. T. Shock Tube Study of the Reaction H + O_2 → OH + O Using OH Laser Absorption. *J. Phys. Chem.* **1990**, *94*, 7119-7128.

[11]Yuan, T.; Wang, C.; Yu, C.-L.; Frenklach, M.; Rabinowitz, M. J. Determination of the Rate Coefficient for the Reaction Hydrogen Atom + Oxygen → Hydrogen + Oxygen Atom by a Shock Tube/Laser Absorption/Detailed Modeling Study. *J. Phys. Chem.* **1991**, *95*, 1258-1265.

[12]Shin, K. S.; Michael, J. V. Rate Constants for the Reactions H + O_2 → OH + O and D + O_2 → OD + O over the Temperature Range 1085–2278 K by the Laser Photolysis–Shock Tube Technique. *J. Chem. Phys.* **1991**, *95*, 262-273.

[13]Du, H.; Hessler, J. P. Rate Coefficient for the Reaction H + O_2 → OH + O: Results at High Temperatures, 2000 To 5300 K. *J. Chem. Phys.* **1992**, *96*, 1077-1092.

[14]Hwang, S. M.; Ryu, S.-O.; Witt, K. J.; Rabinowitz, M. J. High Temperature Rate Coefficient Measurements of H+O_2 Chain-Branching and Chain-Terminating Reaction. *Chem. Phys. Letters* **2005**, *408*, 107-111.

[15]Hong, Z.; Davidson, D. F.; Barbour, E. A.; Hanson, R. K. A New Shock Tube Study of the H + O_2 → OH + O Reaction Rate Using Tunable Diode Laser Absorption of H_2O Near 2.5 μm. *Proc. Combust. Inst.* **2010**, *33*, 309-316.

[16]Varandas, A. J. C.; Brandao, J.; Quintales, L. A. M. A Realistic Hydroperoxo ($HO_2(\widetilde{X}\,^2A''$) Potential Energy Surface from the Double Many-Body Expansion Method. *J. Phys. Chem.* **1988**, *92*, 3732-3742.

[17]Quintales, L. A. M; Varandas, A. J. C; Alvarino, J. M. 1988. "Quintales, L. A. M; Varandas, A. J. C; Alvarino, J. M.. Quasi-Classical Trajectory Calculations of Thermal Rate for the O + OH → O_2 + H Reaction on Realistic Double Many-Body Expansion Potential-Energy Surface for Ground-State HO_2. *J. Phys. Chem.* **1988**, *92*, 4552-4555.

[18]Varandas, A. J. C. Excitation-Function for H + O_2 Reaction – a Study of Zero-Point Energy Effect and Rotational Distributions in Trajectory Calculations, *J. Phys. Chem.* **1993**, *99*, 1076-1085.

[19]Xie, D.; Xu, C.; Ho, T.-S.; Rabitz, H.; Lendvay, G.; Lin, S. Y.; Guo, H. Global Analytical Potential Energy Surfaces for $HO_2(X^2A'')$ Based on High Level Ab Initio Calculations, *J. Chem. Phys.* **2007**, *126*, 074315- 074323.

[20]Harding, L. B.; Maergoiz, A. I.; Troe, J.; Ushakov, V. G. Statistical Rate Theory for the HO + O ⇔ HO_2 ⇔ H + O_2 Reaction System: SACM/CT Calculations Between 0 and 5000 K. *J. Chem. Phys.* **2000**, *113*, 11019-11034.

[21]Troe, J.; Ushakov, V. G. Theoretical Studies of the HO + O ⇔ HO_2 ⇔ H + O_2 Reaction. II. Classical Trajectory Calculations on an Ab Initio Potential for Temperatures Between 300 and 5000 K. *J. Chem. Phys.* **2001**, *115*, 3621-3628.

[22]Harding, L. B.; Troe, J.; Ushakov, V. G. Classical Trajectory Calculations of the High Pressure Limiting Rate Constants and of Specific Rate Constants for the Reaction H + O_2 →

HO_2: Dynamic Isotope Effects Between Tritium+ O_2 and Muonium+ O_2. *Phys. Chem. Chem. Phys.* **1999**, *2*, 631-642.

[23]Michael, J. V.; Sutherland, J. W.; Harding, L. B.; Wagner, A. F. Initiation in H_2/O_2: Rate Constants for $H_2 + O_2 \rightarrow H + HO_2$ at High Temperature. *Proc. Comb. Inst.* **2000**, *28*, 1471–1478.

[24]Troe, J. The Struggle for Precise Rate Constants in Gas Phase Reaction Kinetics: the Reaction $H + O_2 \Leftrightarrow HO + O$. *Z. Phys. Chem.* **2003**, *217*, 1303–1317.

[25]Lendvay, G.; Xie, D.; Guo, H.; Mechanistic Insights into the $H + O_2 \rightarrow OH + O$ Reaction from Quasi-Classical Trajectory Studies on a New Ab Initio Potential Energy Surface, *Chem. Phys.* **2008**, *349*, 181–187.

[26]Sun, Z.; Zhang, D. H.; Xu, C.; Zhou, S.; Xie, D.; Lendvay, G.; Lee, S.-Y.; Lin, S.Y.; Guo, H. State-to-State Dynamics of $H + O_2$ Reaction, Evidence for Nonstatistical Behavior, *J. Am. Chem. Soc.* **2008**, *130*, 14962-14963.

[27]Guo, H. Quantum Dynamics of Complex-Forming Reactions. *Int. Rev. Phys. Chem.* **2012**, *31*, 1-68.

[28]Lin, S. Y.; Guo, H.; Honvault, P.; Xie, D. Quantum Dynamics of the $H + O_2 \rightarrow O + OH$ Reaction on an Accurate Ab Initio Potential Energy Surface. *J. Phys. Chem. B.* **2006**, *110*, 23641-23643.

[29]Honvault, P.; Lin, S. Y.; Xie, D.; Guo, H. Differential and Integral Cross Sections for the $H + O_2 \rightarrow HO + O$ Combustion Reaction. *J. Phys. Chem. A.* **2007**, *111*, 5349-5352.

[30]Lin, S. Y.; Sun, Z.; Guo, H.; Zhang, D. H.; Honvault, P.; Xie, D.; Lee, S.-Y. Fully Coriolis Coupled Quantum Studies of the H + O_2 (v_i=0-2, j_i=0,1) → OH + O Reaction on an Accurate Potential Energy Surface: Integral Cross Sections and Rate Constants. *J. Phys. Chem. A.* **2008**, *112*, 602-611.

[31]Brown, R. L. An Upper Limit for the Rate of Destruction of $O_2(^1\Delta_g)$ by Atomic Hydrogen, *J. Geophys. Res. Space Phys.* **1970**, *75*, 3935-3936.

[32]Westenberg, A. A.; Roscoe, J. M.; DeHaas, N. Rate measurement on N + $O_2(a^1\Delta_g)$ → NO + O and H + $O_2(a^1\Delta_g)$ → OH +O. *Chem. Phys. Lett.* **1970**, *7*, 597-599.

[33]Schmidt, C.; Schiff, H. I. Reactions of Singlet Oxygen with atomic Nitrogen and Hydrogen, *Chem. Phys. Lett.* **1973**, *23*, 339-342.

[34]Cupitt, L. T.; Takacs, G. A.; Glass G. P. Reaction of Hydrogen Atoms and $O_2(^1\Delta_g)$, *Int. J. Chem. Kinet. 1982*, **14**, 487-497.

[35]Basevich, V. Ya.; Vedeneev, V. I.; Konstanta Skorost'i Reakcii H + $O_2(^1\Delta)$ = OH + O [The Rate Constant of the H + $O_2(^1\Delta)$ = OH + O Reaction] *Khim. Fiz.* **1985**, *4*, 1102-1108.

[36]Hack, W.; Kurzke, H. Kinetic Study of the Elementary Chemical Reaction H($^2S_{1/2}$) + $O_2(^1\Delta_g)$ → OH($^2\Pi$) + O(^{3}P) in the Gas Phase, *J. Phys. Chem.* **1986**, *90*, 1900-1906.

[37] Li, A.; Xie, D.; Dawes, R.; Jasper, A. W.; Ma, J.; Guo, H. Global Potential Energy Surface, Vibrational Spectrum, and Reaction Dynamics of the First Excited (A^2A') State of HO_2, *J. Chem. Phys.* **2010**, *133*, 144306-144314.

[38]Ma, J.; Guo, H.; Xie, C.; Li, A.; Xie, D. State-to-state Quantum Dynamics of the $H(^2S)$ + $O_2(a^1\Delta_g) \rightarrow O(^3P)$ + $OH(X^2P)$ Reaction on the First Excited State of $HO_2(A^2A')$. *Phys. Chem. Chem. Phys.* **2011**, *13*, 8407-8413.

[39]Szabó, P.; Lendvay G. A Quasiclassical Trajectory Study of the Reaction of H Atoms with $O_2(^1\Delta_g)$, *J. Phys. Chem. A* **2015**, *119*, 7180-7189.

[40]Lin, S. Y.; Xie, D.; Guo, H. Revelation of Non-Statistical Behavior in HO_2 Vibration by a New Ab Initio Potential Energy Surface, *J. Chem. Phys.* **2006**, *125*, 091103-091103-4.

[41] Bargueno, P.; Gonzalez-Lezana, T.; Larregaray, P.; Bonnet, L.; Rayez, J.-C. Time Dependent Wave Packet and Statistical Calculations on the H + O_2 Reaction *Phys. Chem. Chem. Phys.* **2007**, *9*, 1127-1137.

[42] P. Bargueno, T. Gonzalez-Lezana, P. Larregaray, L. Bonnet, J.-C. Rayez, M. Hankel, S. C. Smith and A. J. H. M. Meijer, Study of the H+O_2 Reaction by Means of Quantum Mechanical and Statistical Spproaches: The Dynamics on Two Different Potential Energy Surfaces, *J. Chem. Phys.*, **2008**, *128*, 244308.

[43] Lin, S. Y.; Guo, H.; Lendvay, G.; Xie, D., Effects of Reactant Rotational Excitation on H + O_2 -> OH + O Reaction Rate Constant: Quantum Wave Packet, Quasi-classical Trajectory and Phase Space Theory Calculations, *Phys. Chem. Chem. Phys.*, **2009**, *11*, 4715–4721.

[44] Hase W. L., Duchovic R. J., Lu D.-H., Swamy K. N., Vande Linde S. R., Wolf R. J.; VENUS, a General Chemical Dynamics Computer Program; 1988.

[45] Xu, C.; Xie, D.; Zhang, D. H.; Lin, S. Y.; Guo, H. A New Ab Initio Potential-energy Surface of $HO_2(X^2A\square\square)$ and Quantum Studies of HO_2 Vibrational Spectrum and Rate Constants for the H+O_2 -> O+OH Reactions *J. Chem. Phys.* **2005**, *122*, 244305.

[46] Perry, R. J.; Dawes R.; Wagner A. F.; Thompson D.L.; A Classical Trajectory Study of the Intramolecular Dynamics, Isomerization, and Unimolecular Dissociation of HO_2, *J. Chem. Phys.*, **2013**, *139*, 084319.

[47]Banares, L.; Aoiz, F. J.; Honvault, P.; Bussery-Honvault, B., Launay, J.-M. Quantum Mechanical and Quasi-classical Trajectory Study of the $C(^1D) + H_2$ Reaction Dynamics *J. Chem. Phys.* **2003**, *118*, 565-568.

[48]Bonnet, L.; Rayez, J.-C. Quasiclassical Trajectory Method for Molecular Scattering Processes: Necessity of a Weighted Binning Approach, *Chem. Phys. Lett.* **1997**, *277*, 183-190.

[49]Bonnet, L.; Rayez, J.-C. Gaussian Weighting in the Quasiclassical Trajectory Method, *Chem. Phys. Lett.* **2004**, *397*, 106-109.

[50] Smith, F. T. Lifetime Matrix in Collision Theory *Phys. Rev.* **1960**, *118*, 349-376, Erratum *Phys. Rev.* **1960**, *119*, 2098.

[51] Clary D.C.; Connor J.N.L; Southall, W.J.E, Reactions of $O(^3P)$ with Saturated Hydrocarbons: Vibrationally Adiabatic Distorted Wave Calculations of Product Rotational Distributions for Two Triatomic Model Reactions, *J. Chem. Phys.* **1986**, *85*, 2620-2623

[52] Troya D.; Lendvay G.; González M.; Schatz G.C. A Quasiclassical Trajectory Study of Angular and Internal State Distributions in $H+H_2O$ and $H+D_2O$ at E_T =1.4eV, *Chem. Phys.Lett.* **2001**, *43*, 420-428.

[53] Barnes P.W.; Sims I.R.; Smith I.W.M.; Lendvay, G.; Schatz G.C. The Branching Ratio between Reaction and Relaxation in the Removal of H_2O from its $|04\rangle^-$ Vibrational State in Collisions with H Atoms *J. Chem. Phys.* **2001**, *115*, 4586-4592.

[54] Johnson B. R., On the Adiabatic Invariance Method of Calculating Semiclassical Eigenvalues, *J. Chem. Phys.*, **1985**, *83*, 1204-1217.